Hyperthermal velocity distributions of recombinatively-desorbing oxygen from Ag(111)

Arved C. Dorst[1,2], Rasika E. A. Dissanayake[1,2], Daniel Schauermann[1], Sofie Knies[3], Alec M. Wodtke[1,2], Daniel R. Killelea[4] and Tim Schäfer[1,2]*

[1]Institute of Physical Chemistry, University of Göttingen, Göttingen, Germany, [2]Max-Planck Institute for Multidisciplinary Sciences, Göttingen, Germany, [3]Faculty of Biology, Chemistry and Geosciences and Bavarian Center for Battery Technology, Bayreuth, Germany, [4]Department of Chemistry and Biochemistry, Loyola University Chicago, Chicago, IL, United States

This study presents velocity-resolved desorption experiments of recombinatively-desorbing oxygen from Ag (111). We combine molecular beam techniques, ion imaging, and temperature-programmed desorption to obtain translational energy distributions of desorbing O_2. Molecular beams of NO_2 are used to prepare a p (4 × 4)-O adlayer on the silver crystal. The translational energy distributions of O_2 are shifted towards hyperthermal energies indicating desorption from an intermediate activated molecular chemisorption state.

KEYWORDS

oxygen, silver, ion imaging, TPD, velocity-resolved, molecular beams, angular distribution, energy distribution

1 Introduction

Silver surfaces play important roles in large scale industrial heterogeneous catalytic processes such as partial oxidation of methanol to formaldehyde and ethylene to ethylene oxide (Serafin et al., 1998; Qian et al., 2003). Because of the tremendous scale of these applications, seemingly modest improvements in the reaction process may lead to big economical and ecological improvements. Therefore, this system has attracted significant attention over the years and numerous studies have focused on the microscopic details of oxidized silver surfaces. Oxygen induced reconstructions of silver surfaces have been thoroughly investigated using high-precision ultra-high vacuum (UHV) surface science techniques in combination with theoretical approaches (Bao et al., 1996; Michaelides et al., 2005; Schnadt et al., 2006; Greeley and Mavrikakis, 2007; Reichelt et al., 2007; Rocha et al., 2012; Martin et al., 2014; Jones et al., 2015a; Jones et al., 2015b). Ag (111) exhibits a variety of different reconstructed surfaces with similar stability which have been studied and discussed for many years. A detailed review about the history of considered oxygen structures on Ag (111) is given by Michaelides et al. (2005).

Experimentally, the oxidation of Ag (111) under UHV conditions with molecular oxygen is difficult due to the low sticking probability (ca. 1×10^{-6}) of O_2 (Campbell, 1985; Kleyn et al., 1996). In early UHV studies, silver surfaces were therefore oxidized under comparatively high O_2 pressures before characterization under UHV conditions (Campbell, 1985). The use of more aggressive oxidants circumvents this issue; in particular, atomic oxygen (Bukhtiyarov et al., 2003; Böcklein et al., 2013; Derouin et al.,

2015) or NO$_2$ (Bare et al., 1995; Huang and White, 2003) allow for silver surface oxidation under UHV compatible conditions. When using NO$_2$ as oxidant, the temperature range at which clean oxidized surfaces are produced is restricted between ca. 490 K and 520 K since at lower temperatures NO$_2$ adsorbs molecularly and at elevated temperatures, O$_2$ starts desorbing (Huang and White, 2003). When oxidizing at these temperatures, the reconstructed surface is indistinguishable from surfaces oxidized with molecular oxygen and consists mainly out of p (4 × 4)-O domains (Carlisle et al., 2000a; Carlisle et al., 2000b). In contrast, oxidizing with atomic oxygen is possible at lower temperatures. It typically results in slightly different surface phases and forms subsurface oxygen below 510 K, (Derouin et al., 2015).

The large number of reconstructed oxidized Ag (111) surfaces observed in experiments has motivated theory groups to develop models describing surface stability based on first principles theory (Michaelides et al., 2003; Li et al., 2003a,b; Michaelides et al., 2005). Using *ab initio* thermodynamics and first principles simulations, theory is able to provide (T, p) phase diagrams describing stable oxidized surface phases from UHV to high pressure conditions present at real world catalysts (Reuter, 2016). By comparison with experimental results, microscopic details of the oxidized surface structure can be elucidated.

Additional theoretical work has focused on the dynamics of the O$_2$ dissociation process on Ag (111). These studies do not aim for clarifying the geometry of reconstructed surfaces but provide theoretical data on the atomic scale mechanism of the oxidation process itself (Xu et al., 2005; Kunisada et al., 2011; Kunisada and Sakaguchi, 2014). Kunisada and Sakaguchi investigated quantum dynamics of O$_2$/Ag (111) dissociative adsorption propagating on a six-dimensional potential energy surface (PES) obtained from density-functional theory (DFT) (Kunisada and Sakaguchi, 2014). From the PES, they identify the lowest barrier near a top site with a height of 1.37 eV. Coupled-channel calculations trajectories based on this PES provide dissociation probabilities for O$_2$ as function of the incident translational and vibrational energy. Interestingly, dissociation occurs even with translational energies slightly below the activation barrier height, which the authors explain by O$_2$ tunneling effects. The computations also show a significant dissociation enhancement by increasing the incident vibrational energy caused by a late barrier in the reaction pathway. In another theoretical study based on a neural network interpolated PES, Goikoetxea et al. investigated electronically non-adiabatic effects during the dissociative adsorption of O$_2$ at Ag (111) (Goikoetxea et al., 2012). They also identified a large energy barrier for dissociation above 1 eV close to the surface. As non-adiabatic effects affect sticking probabilities at elevated distances to the surface and are expected to be smaller than the adiabatic energy barrier, their influence on the sticking probability is negligible.

Such theoretical work provides excellent data for comparison with surface dynamics experiments under well-controlled UHV conditions. A classical experimental approach probes the entrance channel of the reaction pathway by employing pulsed molecular beams of reactants to initiate the surface reaction (Barker and Auerbach, 1984; Kleyn et al., 1996; Sitz, 2002; Kleyn, 2003; Golibrzuch et al., 2015; Chadwick and Beck, 2016; Vattuone and Okada, 2020; Shen et al., 2022). Seeding reactants in different carrier gases allows for modification of the incident translational

energy. Incident vibrational energy can be altered by thermal or laser excitation. Surface reactivity as function of varied incident parameters is probed using, for instance, Meitner-Auger electron spectroscopy (MAES) or temperature -programmed desorption (TPD) for coverage determination after exposing the surface for a selected time to a molecular beam.

Surface reaction dynamics experiments on the exit channel probe degrees of freedom of the desorbing reaction products using quantum state-resolved detection methods in combination with translational energy dependent measurements (Comsa and David, 1982; Michelsen and Auerbach, 1991; Michelsen et al., 1992; Shuai et al., 2017; Kaufmann et al., 2018; Dorst et al., 2022). From these studies, translational, rotational, and vibrational state distributions of products can be deduced. Eventually, concepts of detailed balance allow to model these distributions and to defer quantitative heights of reaction barriers.

Recently, we used this approach to investigate the recombinative desorption of oxygen from Rh (111) (Dorst et al., 2022). O$_2$ was detected using a velocity map imaging (VMI) setup after non-resonant ionization with a femtosecond pulse of 800 nm. The desorption process was initiated by linearly heating the sample in a TPD type approach. We identified hyperthermal velocity distributions for oxygen molecules desorbing from surface sites as well as for oxygen molecules originating from subsurface, indicating a common intermediate desorption state.

In this paper, we present angular distributions and translational energy distribution of recombinatively-desorbing O$_2$ from Ag (111). We prepare p (4 × 4)-O Ag (111) by dosing the surface with a molecular beam of NO$_2$ seeded in rare gases at a surface temperature of 510 K. Angular distributions are narrow and hyperthermal translational energy distributions indicate an activated desorption process.

2 Experimental

The experimental setup has been previously described in detail (Westphal et al., 2020). Briefly, experiments were conducted under ultra-high vacuum (UHV) conditions at a base pressure of <5 × 10^{-10} mbar. We dose the surface with a pulsed supersonic molecular beam of 10% NO$_2$ (AirLiquide, 99.5%) seeded in He (AlphaGaz, ≥99.999%) using a home-built pulsed solenoid nozzle (Park et al., 2016). During exposure, we maintain UHV conditions by differential pumping techniques.

For surface cleaning, the UHV apparatus is equipped with an ion gun (Staib Instruments IG-5-C), with which the surface is Ar$^+$-sputtered (2.00 kV, 2.0 × 10^{-7} mbar Ar) for multiple cycles. After annealing (700 K, 30 min), the surface cleanliness is checked by Meitner-Auger electron spectroscopy (OCI BDL 450) and low-energy electron diffraction (LEED) spectroscopy (OCI BDL 450). The Ag (111) crystal (MaTecK, 99.99%, ∅ 10 mm, 2 mm thickness) is mounted on a home-built sample holder and is resistively heated by Ta filaments; temperatures are monitored by a K-type thermocouple. With liquid nitrogen cooling, the accessible temperatures range from 100 K to 1,235 K. We use a home-written LabVIEW™ program for data acquisition and control of experimental parameters.

Velocity distributions of surface desorption products are obtained by combining velocity map imaging (VMI) and
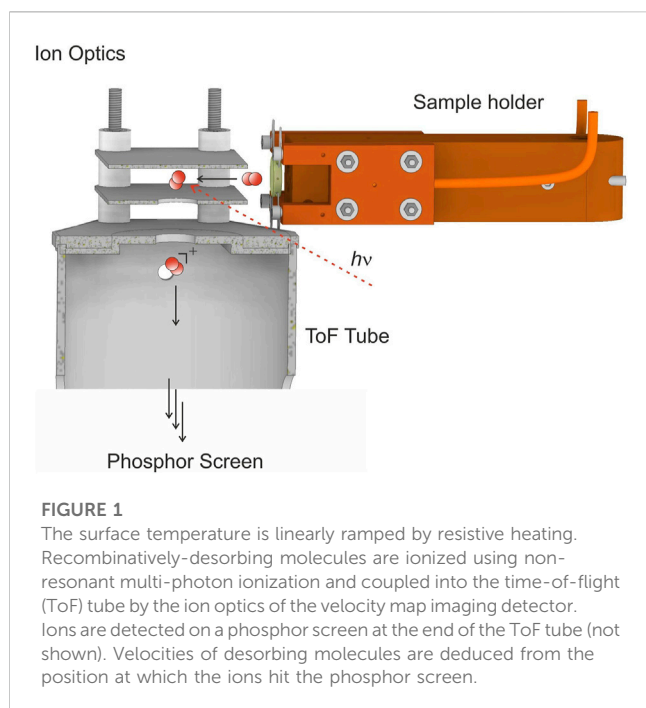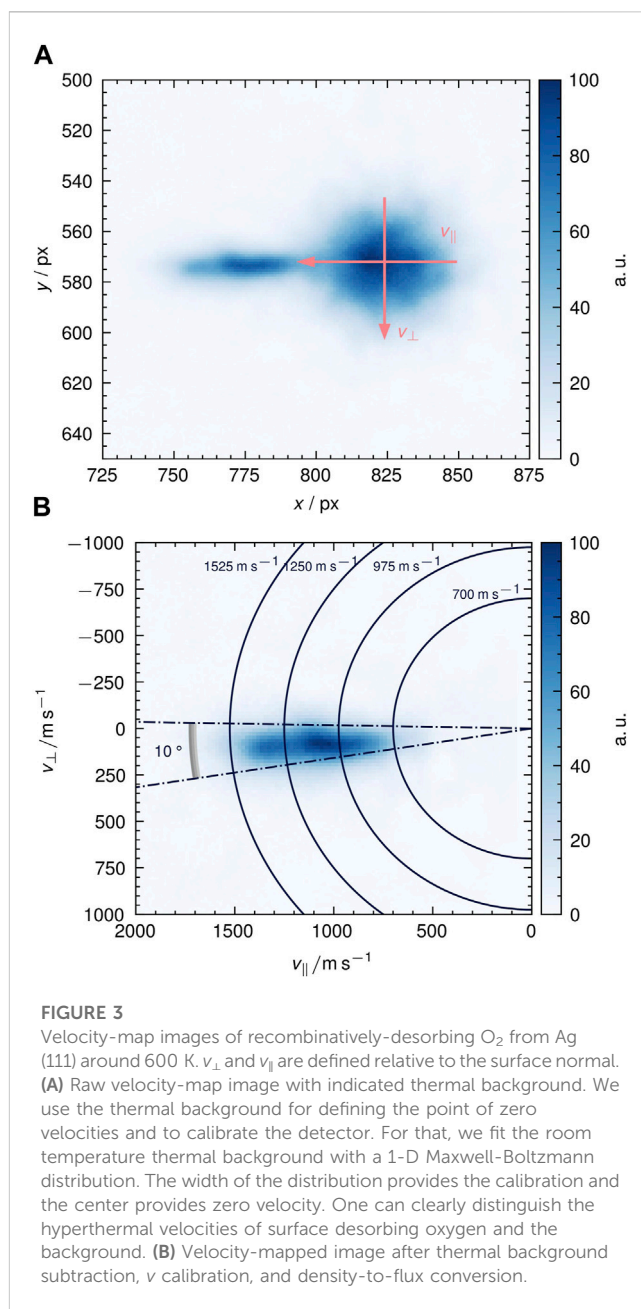
FIGURE 1
The surface temperature is linearly ramped by resistive heating. Recombinatively-desorbing molecules are ionized using non-resonant multi-photon ionization and coupled into the time-of-flight (ToF) tube by the ion optics of the velocity map imaging detector. Ions are detected on a phosphor screen at the end of the ToF tube (not shown). Velocities of desorbing molecules are deduced from the position at which the ions hit the phosphor screen.
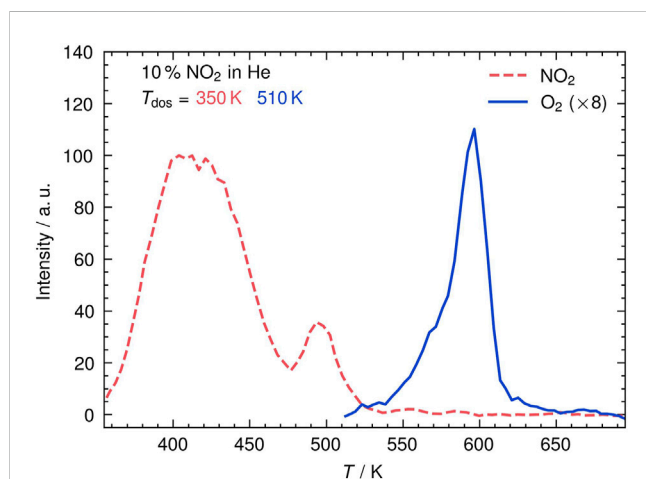
FIGURE 2
VMI-TPD spectrum of desorbing NO_2 (dashed) and recombinatively-desorbing O_2 (solid) after identical NO_2 exposure of an Ag (111) surface. The integrated flux density is plotted as a function of the temperature T; T_{dos} is the dosage temperature.

FIGURE 3
Velocity-map images of recombinatively-desorbing O_2 from Ag (111) around 600 K. $v_\perp$ and $v_\parallel$ are defined relative to the surface normal. **(A)** Raw velocity-map image with indicated thermal background. We use the thermal background for defining the point of zero velocities and to calibrate the detector. For that, we fit the room temperature thermal background with a 1-D Maxwell-Boltzmann distribution. The width of the distribution provides the calibration and the center provides zero velocity. One can clearly distinguish the hyperthermal velocities of surface desorbing oxygen and the background. **(B)** Velocity-mapped image after thermal background subtraction, v calibration, and density-to-flux conversion.

temperature-programmed desorption (TPD) experiments: we linearly heat up the surface while simultaneously detecting velocity map images of desorbing molecules. For that, the beam of a regeneratively amplified femtosecond laser (Spectra-Physics, Solstice Ace, <35 fs, 800 nm, 1 kHz) is focused by an optical lens (f = 300 mm) such that molecules are non-resonantly ionized after desorption. The ions are detected by an imaging setup which follows the design by Eppink and Parker (Eppink and Parker, 1997). Micro-channel plates (MCPs, Topag, MCP 56–15) are used for signal amplification and ions are imaged using a CMOS camera (Basler ace acA 1,920–155 µm, 1,920 px × 1,200 px) recording the images from a phosphor screen (Proxivision P43). Figure 1 shows the ionization region of the experimental setup.

Before each TPD experiment, the sample is exposed to the molecular beam at a defined dosage temperature. Afterwards, the surface is linearly heated at 4 K s^{-1} in a TPD experiment while we record images at 1 kHz laser repetition rate.

3 Results and discussion

For investigating velocity-resolved desorption of recombinatively-desorbing oxygen, we first create a complete monolayer of a p (4 × 4)-O phase on Ag (111) by dosing it with NO_2 from a molecular beam at T_{surf} = 350 K or 510 K for 2 min at a
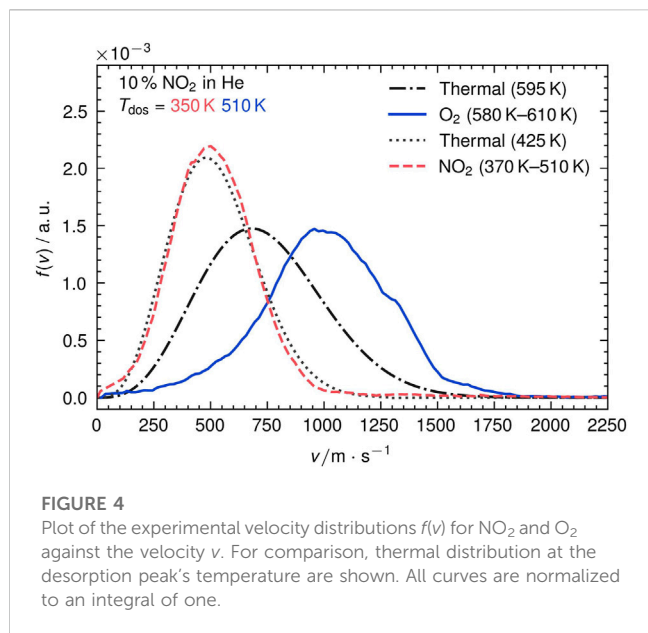
FIGURE 4
Plot of the experimental velocity distributions $f(v)$ for NO_2 and O_2 against the velocity v. For comparison, thermal distribution at the desorption peak's temperature are shown. All curves are normalized to an integral of one.

TABLE 1 Mean experimental velocities $\langle v \rangle$, energies $\langle E \rangle$, and the corresponding mean thermal velocities $\langle v_{th} \rangle$ for a desorption temperature $\langle T \rangle$ of desorbing NO_2 and recombinatively-desorbing O_2 from Ag (111).

Compound	$\langle T \rangle$/K	$\langle v \rangle$/m s^{-1}	$\langle v_{th} \rangle$/m s^{-1}	$\langle E \rangle$/eV
NO_2	425	530	520	0.0731
O_2	595	1,010	795	0.186

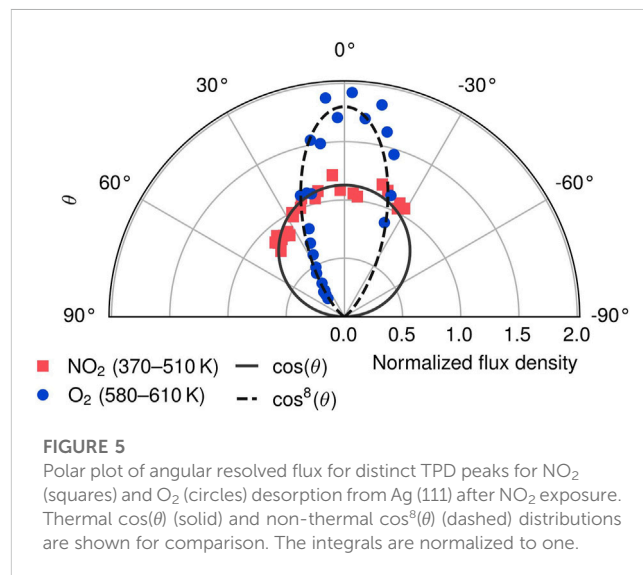**FIGURE 5**
Polar plot of angular resolved flux for distinct TPD peaks for NO_2 (squares) and O_2 (circles) desorption from Ag (111) after NO_2 exposure. Thermal $\cos(\theta)$ (solid) and non-thermal $\cos^8(\theta)$ (dashed) distributions are shown for comparison. The integrals are normalized to one.

nozzle frequency of 200 Hz. We check the degree of oxidation by LEED and TPD (see Supplementary Material). Depending on the surface temperature during exposure, either nitrate (NO_3) or pure oxygen layers may form (Alemozafar and Madix, 2005). In Figure 2, we show TPD spectra of NO_2 and O_2 recorded with the VMI setup displayed in Figure 1. We record the total signal at the phosphor screen of the molecular mass of the parent ion by gating the phosphor screen to the respective time-of-flight. The VMI-TPD spectrum of NO_2 (dashed curve) shows two different desorption features after dosing at 350 K: first, a broad desorption peak ranging up to 470 K followed by a less broad, lower intensity desorption between 480 K and 510 K. These features are attributed to NO_3 decomposition into NO_2(g) and O from two different states (Alemozafar and Madix, 2005). In contrast, O_2 (solid curve) desorbs at significantly higher temperatures at T_{surf} of $\approx$590 K (Huang and White, 2003).

We use the VMI setup to determine velocity distributions for both, desorbing NO_2 and recombinatively-desorbing O_2. Figure 3A shows the raw image of O_2 desorption from Ag (111) around 590 K. We obtain the image by averaging all images that we record during a desorption peak in a TPD run. The raw image clearly displays the residual thermal gas background in the UHV chamber as circular spot as indicated in Figure 3A. From the background we deduce the point of zero velocity. We further calibrate the detector by fitting a one-dimensional Maxwell-Boltzmann distribution to the thermal background. Figure 3B shows the calibrated figure after subtraction of the thermal background and density-to-flux conversion (Harding et al., 2017). The velocity-mapped image shows a directed desorption feature with hyperthermal velocities between 500 m s^{-1} and 1,500 m s^{-1}. The angular tilt is due to a slightly tilted suspension of the crystal in the sample holder. From such images, we deduce velocity distributions by iterative integration over velocity increments within $10°$-broad angular slices as shown in Figure 3B. In Figure 4, we show the results for the NO_2 peak at 425 K and the O_2 peak at 595 K. All curve integrals are

normalized to unity. For comparison, thermal flux-weighted Maxwell-Boltzmann distributions of the shape

$$f(v, T_{surf}) \propto v^3 \cdot \exp\left(-\frac{M \cdot v^2}{R \cdot T_{surf}}\right) \qquad (1)$$

are plotted. M denotes the molar mass of the compounds and R is the universal gas constant. We use the signal-weighted temperature $\langle T \rangle$ of 425 K for NO_2 and 595 K for O_2 for T_{surf}.

From the figure it is obvious that O_2 desorbs with hyperthermal velocities indicated by a shift of the curve's maximum by more than 300 m s^{-1} compared to a flux-weighted thermal velocity distribution. In contrast, NO_2 desorption is clearly thermal as it can be well-reproduced by a flux-weighted Maxwell-Boltzmann distribution of the surface temperature. We did not observe any significant difference between the two desorption features of NO_3 decomposition (see Supplementary Material). Table 1 lists the characteristic properties of the shown velocity distributions.

Additionally, we record angular distributions of NO_2 and O_2 desorption from Ag (111). For that, we move the surface parellel to the detector such that only molecules from certain desorption angles are detected as described previously (Dorst et al., 2022). As VMI provides the direction of velocities in the detector plane, desorption angles are directly obtained from the ion images. Figure 5 shows a polar plot of the angular resolved flux for both, NO_2 (squares) and O_2 (circles) desorption. For comparison, a $\cos(\theta)$-distribution is shown, which would be expected for thermal desorption. We observe a narrow $\cos^8(\theta)$-angular distribution for O_2 desorption, whereas NO_2 desorption resembles the $\cos(\theta)$-distribution indicative of a thermalized (or equilibrium) desorption process.
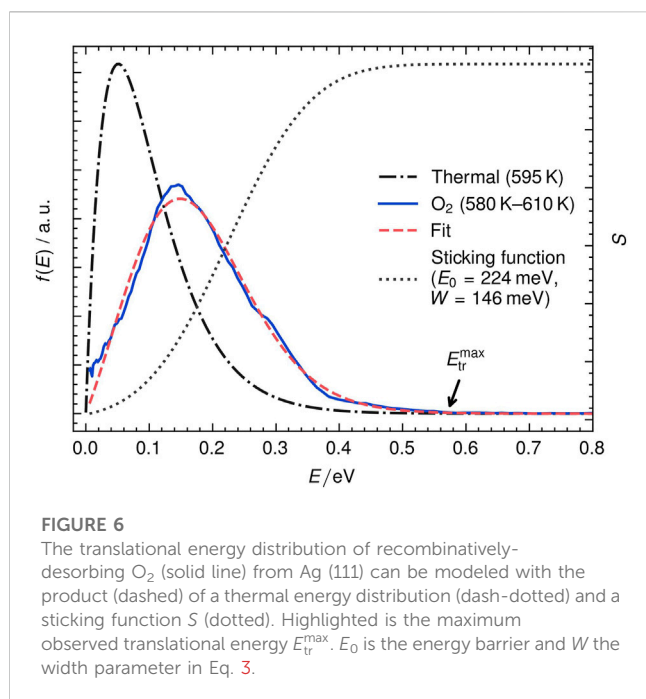
FIGURE 6
The translational energy distribution of recombinatively-desorbing O_2 (solid line) from Ag (111) can be modeled with the product (dashed) of a thermal energy distribution (dash-dotted) and a sticking function S (dotted). Highlighted is the maximum observed translational energy E_{tr}^{max}. E_0 is the energy barrier and W the width parameter in Eq. 3.

From the presented desorption dynamics, details of the underlying potential energy surface (PES) are obtained. The narrow angular distribution of O_2 desorption indicates an activated desorption process. Molecules have to overcome a barrier, on which they get accelerated into the gas phase. This is known to result in very peaked angular distributions (Comsa and David, 1985). In contrast, the release of NO_2 after surface nitrate decomposition appears with a broad angular distribution, indicating a non-activated thermalized desorption process.

Also, velocities of desorbing molecules provide valuable information about the underlying PES. Figure 6 shows the translational energy distribution of recombinatively-desorbing O_2 from Ag (111). The distributions are obtained from the velocity distributions displayed in Figure 4. The O_2 distribution is clearly shifted towards higher energies; NO_2 resembles a thermal distribution.

The shift of the hyperthermal O_2 energy distribution can be used to quantify energy-dependent sticking probabilities using the concepts of detailed balance (White and Beuhler, 2004). In an activated adsorption process, an energy barrier in the adsorption trajectory suppresses sticking at low incident translational energies. As a consequence, molecules with low translational energy are missing in translational energy distributions of desorption (Comsa and David, 1982; Michelsen and Auerbach, 1991; Shuai et al., 2017; Kaufmann et al., 2018). Following the principles of detailed balance, we can fit the hyperthermal distribution in Figure 6 using the product of a flux-weighted thermal energy distribution and a sticking function (see Eq. 2).

$$f(E_{tr}, T_{surf}) = K \cdot E_{tr} \cdot \exp\left(-\frac{E_{tr}}{k_B \cdot T_{surf}}\right) \cdot S(E_{tr}) \quad (2)$$

Here, K is a constant factor, E_{tr} is the translational energy of desorbing molecules, T_{surf} is the surface temperature and $S(E_{tr})$ is the sticking function. We apply an error function to describe sticking (see Eq. 3) as has been done in previous studies for activated adsorption processes

and plot the sticking function in Figure 6 as dashed lines (Michelsen and Auerbach, 1991; Michelsen et al., 1992; Luntz, 2000).

$$S(E_{tr}) = \frac{1}{2}\left(1 + erf\left(\frac{E_{tr} - E_0}{W}\right)\right) \quad (3)$$

W represents the width and E_0 represents the inflection point. We fit our data with a $E_0 = 0.224$ eV as shown in Figure 6. Not that the inflection point corresponds to the onset of adsorption and is related to the energy barrier height. This height is often strongly dependent on the adsorbate's rotational and vibrational state. State-resolved permeation studies on energy distributions of the H_2/Cu(111) system reveal for instance significant enhanced sticking probabilities for vibrationally excited molecules (Michelsen and Auerbach, 1991). However, in this work, we universally ionize desorption products without quantum state resolution. The translational energy distribution should therefore be considered as an averaged distribution of different states with unknown populations. We define also the maximum observable O_2 translational energy E_{tr}^{max} similar to the method developed by Fingerhut et al. (2021). In their work on formate decomposition on hydrogenated Pt (111), they identified E_{tr}^{max} as lower limit of the energy barrier in the entrance channel.

We indicate this threshold as black arrow in Figure 6 at ca. 0.57 eV ($\approx$1850 m s^{-1}). For these fast molecules, we assume no internal energy and that the recoil against the surface from the transition state results only in minor Ag phonon excitation. This value should therefore be the lower limit to the real energy barrier height as we do not account for excitation of the solid.

Interestingly, these values are significantly lower than calculated sticking probabilities based on first principles theory (Goikoetxea et al., 2012; Kunisada and Sakaguchi, 2014). Kunisada and Sakaguchi calculate state-resolved sticking by performing quantum dynamics calculations of O_2 dissociative desorption on Ag (111) on a before computed PES (Kunisada et al., 2011). Depending on the adsorption site, they predict the onset of adsorption between 1.2 eV and 2.1 eV O_2 incident energy. They also calculate a significant influence of vibrational excitation on the dissociation probability by reducing the onset by ca. 30% when comparing O_2 ($v = 0$) to O_2 ($v = 3$). However, this reduction is still not sufficient to explain the discrepancy between the experimentally measured onset of this study of 0.57 eV and the minimum value of 0.8 eV (O_2 ($v = 3$) for a bridge site) of the theoretical work. We therefore suspect that we do not map a direct dissociation trajectory but desorption from another intermediate surface state under the experimental conditions applied in this study.

In a systematic molecular beam surface scattering approach, Kleyn et al. studied the interaction of O_2 molecular beams with Ag (111) at 150 K identifying several scattering pathways using ToF detection techniques (Raukema and Kleyn, 1995; Kleyn et al., 1996; Raukema et al., 1997). From the ToF of scattered O_2, translational energy distributions are obtained, which can be attributed to different surface states prior to desorption. In general, for the O_2/Ag (111) system, three adsorption states exist: a shallow physisorption well, a molecular chemisorption well, and a dissociative chemisorbed state (Campbell, 1985). At low incident translational energies, scattered oxygen exhibits low velocities, indicating desorption from the physisorbed state. At elevated incident energies, two significantly faster scattering channels are observed. The fastest channel depends on the incident energy indicating directly scattered O_2. In contrast, the other fast channel is independent on the incident energy, so that the

authors assign this pathway to transient trapping desorption from the molecular chemisorption potential energy well. Adsorption in this state is activated with a threshold mean energy of about 0.2 eV, and exhibits electron transfer from the surface to the adsorbate. The molecular chemisorption state can serve as precursor state for dissociative chemisorption (Kleyn et al., 1996). Recent calculations indicate an energy barrier of 0.8 eV between both states (Hinsch et al., 2021). The mean final energy of O_2 molecules originating from the molecular chemisorption state recorded by Kleyn et al. is 0.14 eV (Kleyn et al., 1996). It is close to 0.19 eV, which we measured in this study. The lower translational energy could be caused by the significant colder surface temperature of 150 K. This is indication that the desorption state, which we observe in TPD experiments at 590 K, is identical to the intermediate molecular chemisorption state observed in molecular beam surface scattering experiments.

4 Conclusion

We performed velocity resolved surface desorption experiments of recombinatively desorbing O_2 from Ag (111) by combining ion imaging techniques with temperature programmed desorption. Desorption occurs at 590 K, is clearly hyperthermal, and exhibits a narrow angular distribution indicating an activated desorption process. Velocity distributions are similar to previously reported distributions from molecular beam surface scattering experiments. For both studies, the energetics of desorbing molecules indicate desorption from an intermediate molecular chemisorption state. Recent theoretical papers calculate significantly higher barriers for oxygen sticking on Ag (111) than we deduce from the translational energy distribution (Kunisada and Sakaguchi, 2014). The here presented data will be a valuable experimental benchmark to refine theoretical models crucial for a better understanding of surface dynamics in metal oxidation processes.

Data availability statement

The raw data supporting the conclusion of this article will be made available by the authors, without undue reservation. It is available under GRO.data (https://data.goettingen-research-online.de/dataverse/hyperthermal_v_distr_desorbing_o2_ag111). Further inquiries can be directed to the corresponding author.

Author contributions

AD performed the experiments, data analysis and wrote a first paper draft. RD performed the experiments and analyzed the data.

DS and SK contributed with experiments. AW contributed with discussion and the conception and design of the research. DK contributed with discussion and writing. TS conceptualized the experiment, analyzed the data and contributed with writing. All authors contributed to the article and approved the submitted version.

Conflict of interest

The authors declare that the research was conducted in the absence of any commercial or financial relationships that could be construed as a potential conflict of interest.

Publisher's note

All claims expressed in this article are solely those of the authors and do not necessarily represent those of their affiliated organizations, or those of the publisher, the editors and the reviewers. Any product that may be evaluated in this article, or claim that may be made by its manufacturer, is not guaranteed or endorsed by the publisher.

Supplementary material

The Supplementary Material for this article can be found online at: https://www.frontiersin.org/articles/10.3389/fchem.2023.1248456/full#supplementary-material

References

Alemozafar, A. R., and Madix, R. J. (2005). The adsorption of and reaction of NO_2 on Ag(111)-*p*(4×4)-O and formation of surface nitrate. *Surf. Sci.* 587, 193–204. doi:10.1016/j.susc.2005.05.019

Bao, X., Muhler, M., Schedel-Niedrig, T., and Schlögl, R. (1996). Interaction of oxygen with silver at high temperature and atmospheric pressure: A spectroscopic and structural analysis of a strongly bound surface species. *Phys. Rev. B* 54, 2249–2262. doi:10.1103/physrevb.54.2249

Bare, S. R., Griffiths, K., Lennard, W. N., and Tang, H. T. (1995). Generation of atomic oxygen on Ag(111) and Ag(110) using NO_2: A TPD, LEED, HREELS, XPS and NRA study. *Surf. Sci.* 342, 185–198. doi:10.1016/0039-6028(95)00670-2

Barker, J. A., and Auerbach, D. J. (1984). Gas-surface interactions and dynamics; thermal energy atomic and molecular beam studies. *Surf. Sci. Rep.* 4, 1–99. doi:10.1016/0167-5729(84)90005-0

Böcklein, S., Günther, S., and Wintterlin, J. (2013). High-pressure scanning tunneling microscopy of a silver surface during catalytic formation of ethylene oxide. *Angew. Chem. Int. Ed.* 52, 5518–5521. doi:10.1002/anie.201210209

Bukhtiyarov, V. I., Hävecker, M., Kaichev, V. V., Knop-Gericke, A., Mayer, R. W., and Schlögl, R. (2003). Atomic oxygen species on silver: Photoelectron spectroscopy and X-ray absorption studies. *Phys. Rev. B* 67, 235422. doi:10.1103/physrevb.67.235422

Campbell, C. T. (1985). Atomic and molecular oxygen adsorption on Ag(111). *Surf. Sci.* 157, 43–60. doi:10.1016/0039-6028(85)90634-x

Carlisle, C. I., Fujimoto, T., Sim, W. S., and King, D. A. (2000a). Atomic imaging of the transition between oxygen chemisorption and oxide film growth on Ag(111). *Surf. Sci.* 470, 15–31. doi:10.1016/s0039-6028(00)00831-1

Carlisle, C. I., King, D. A., Bocquet, M. L., Cerdá, J., and Sautet, P. (2000b). Imaging the surface and the interface atoms of an oxide film on Ag(111) by scanning tunneling microscopy: Experiment and theory. *Phys. Rev. Lett.* 84, 3899–3902. doi:10.1103/physrevlett.84.3899

Chadwick, H., and Beck, R. D. (2016). Quantum state resolved gas–surface reaction dynamics experiments: A tutorial review. *Chem. Soc. Rev.* 45, 3576–3594. doi:10.1039/c5cs00476d

Comsa, G., and David, R. (1985). Dynamical parameters of desorbing molecules. *Surf. Sci. Rep.* 5, 145–198. doi:10.1016/0167-5729(85)90009-3

Comsa, G., and David, R. (1982). The purely fast distribution of H_2 and D_2 molecules desorbing from Cu(100) and Cu(111) surfaces. *Surf. Sci.* 117, 77–84. doi:10.1016/0039-6028(82)90487-3

Derouin, J., Farber, R. G., Heslop, S. L., and Killelea, D. R. (2015). Formation of surface oxides and Ag_2O thin films with atomic oxygen on Ag(111). *Surf. Sci.* 641, L1–L4. doi:10.1016/j.susc.2015.07.003

Dorst, A. C., Güthoff, F., Schauermann, D., Wodtke, A. M., Killelea, D. R., and Schäfer, T. (2022). Velocity map images of desorbing oxygen from sub-surface states of Rh(111). *Phys. Chem. Chem. Phys.* 24, 26421–26427. doi:10.1039/d2cp03369k

Eppink, A. T. J. B., and Parker, D. H. (1997). Velocity map imaging of ions and electrons using electrostatic lenses: Application in photoelectron and photofragment ion imaging of molecular oxygen. *Rev. Sci. Instrum.* 68, 3477–3484. doi:10.1063/1.1148310

Fingerhut, J., Borodin, D., Schwarzer, M., Skoulatakis, G., Auerbach, D. J., Wodtke, A. M., et al. (2021). The barrier for CO_2 functionalization to formate on hydrogenated Pt. *J. Phys. Chem. A* 125, 7396–7405. doi:10.1021/acs.jpca.1c04833

Goikoetxea, I., Beltràn, J., Meyer, J., Juaristi, J. I., Alducin, M., and Reuter, K. (2012). Non-adiabatic effects during the dissociative adsorption of o2 at Ag(111)? A first-principles divide and conquer study. *New J. Phys.* 14, 013050. doi:10.1088/1367-2630/14/1/013050

Golibrzuch, K., Bartels, N., Auerbach, D. J., and Wodtke, A. M. (2015). The dynamics of molecular interactions and chemical reactions at metal surfaces: Testing the foundations of theory. *Annu. Rev. Phys. Chem.* 66, 399–425. doi:10.1146/annurev-physchem-040214-121958

Greeley, J., and Mavrikakis, M. (2007). On the role of subsurface oxygen and ethylenedioxy in ethylene epoxidation on silver. *J. Phys. Chem. C* 111, 7992–7999. doi:10.1021/jp070490i

Harding, D. J., Neugebohren, J., Hahn, H., Auerbach, D. J., Kitsopoulos, T. N., and Wodtke, A. M. (2017). Ion and velocity map imaging for surface dynamics and kinetics. *J. Chem. Phys.* 147, 013939. doi:10.1063/1.4983307

Hinsch, J. J., Liu, J., and Wang, Y. (2021). Reinvestigating oxygen adsorption on Ag(111) by using strongly constrained and appropriately normed semi-local density functional with the revised vydrov van voorhis van der waals force correction. *J. Chem. Phys.* 155, 234704. doi:10.1063/5.0073407

Huang, W. X., and White, J. M. (2003). Revisiting NO_2 on Ag(111): A detailed TPD and rairs study. *Surf. Sci.* 529, 455–470. doi:10.1016/s0039-6028(03)00332-7

Jones, T. E., Rocha, T. C. R., Knop-Gericke, A., Stampfl, C., Schlögl, R., and Piccinin, S. (2015a). Insights into the electronic structure of the oxygen species active in alkene epoxidation on silver. *ACS Catal.* 5, 5846–5850. doi:10.1021/acscatal.5b01543

Jones, T. E., Rocha, T. C. R., Knop-Gericke, A., Stampfl, C., Schlögl, R., and Piccinin, S. (2015b). Thermodynamic and spectroscopic properties of oxygen on silver under an oxygen atmosphere. *Phys. Chem. Chem. Phys.* 17, 9288–9312. doi:10.1039/c5cp00342c

Kaufmann, S., Shuai, Q., Auerbach, D. J., Schwarzer, D., and Wodtke, A. M. (2018). Associative desorption of hydrogen isotopologues from copper surfaces: Characterization of two reaction mechanisms. *J. Chem. Phys.* 148, 194703. doi:10.1063/1.5025666

Kleyn, A. W., Butler, D. A., and Raukema, A. (1996). Dynamics of the interaction of O_2 with silver surfaces. *Surf. Sci.* 363, 29–41. doi:10.1016/0039-6028(96)00089-1

Kleyn, A. W. (2003). Molecular beams and chemical dynamics at surfaces. *Chem. Soc. Rev.* 32, 87–95. doi:10.1039/b105760j

Kunisada, Y., Nakanishi, H., and Kasai, H. (2011). A first principles study of O_2/Ag(111) adsorption and magnetic properties. *J. Phys. Soc. Jpn.* 80, 084605. doi:10.1143/jpsj.80.084605

Kunisada, Y., and Sakaguchi, N. (2014). Two-dimensional quantum dynamics of O_2 dissociative adsorption on Ag(111). *RSC Adv.* 4, 63508–63512. doi:10.1039/c4ra12448k

Li, W. X., Stampfl, C., and Scheffler, M. (2003a). Subsurface oxygen and surface oxide formation at Ag(111): A density-functional theory investigation. *Phys. Rev. B* 67, 045408. doi:10.1103/physrevb.67.045408

Li, W. X., Stampfl, C., and Scheffler, M. (2003b). Why is a noble metal catalytically active? The role of the O-Ag interaction in the function of silver as an oxidation catalyst. *Phys. Rev. Lett.* 90, 256102. doi:10.1103/physrevlett.90.256102

Luntz, A. C. (2000). A simple model for associative desorption and dissociative chemisorption. *J. Chem. Phys.* 113, 6901–6905. doi:10.1063/1.1311280

Martin, N. M., Klacar, S., Grönbeck, H., Knudsen, J., Schnadt, J., Blomberg, S., et al. (2014). High-coverage oxygen-induced surface structures on Ag(111). *J. Phys. Chem. C* 118, 15324–15331. doi:10.1021/jp504387p

Michaelides, A., Bocquet, M. L., Sautet, P., Alavi, A., and King, D. A. (2003). Structures and thermodynamic phase transitions for oxygen and silver oxide phases on Ag(111). *Chem. Phys. Lett.* 367, 344–350. doi:10.1016/s0009-2614(02)01699-8

Michaelides, A., Reuter, K., and Scheffler, M. (2005). When seeing is not believing: Oxygen on Ag(111), a simple adsorption system? *J. Vac. Sci. Technol. A Vac. Surf. Films* 23, 1487–1497. doi:10.1116/1.2049302

Michelsen, H. A., and Auerbach, D. J. (1991). A critical examination of data on the dissociative adsorption and associative desorption of hydrogen at copper surfaces. *J. Chem. Phys.* 94, 7502–7520. doi:10.1063/1.460182

Michelsen, H. A., Rettner, C. T., and Auerbach, D. J. (1992). On the influence of surface temperature on adsorption and desorption in the D_2/Cu(111) system. *Surf. Sci.* 272, 65–72. doi:10.1016/0039-6028(92)91422-8

Park, G. B., Krüger, B. C., Meyer, S., Schwarzer, D., and Schäfer, T. (2016). The ν_6 fundamental frequency of the ã state of formaldehyde and coriolis perturbations in the $3\nu_4$ level. *J. Chem. Phys.* 144, 194308. doi:10.1063/1.4948635

Qian, M., Liauw, M. A., and Emig, G. (2003). Formaldehyde synthesis from methanol over silver catalysts. *Appl. Catal. A* 238, 211–222. doi:10.1016/s0926-860x(02)00340-x

Raukema, A., Butler, D. A., and Kleyn, A. W. (1997). O_2 transient trapping-desorption at the Ag(111) surface. *J. Chem. Phys.* 106, 2477–2491. doi:10.1063/1.473155

Raukema, A., and Kleyn, A. W. (1995). Transient trapping desorption of molecules at surfaces. *Phys. Rev. Lett.* 74, 4333–4336. doi:10.1103/physrevlett.74.4333

Reichelt, R., Günther, S., Wintterlin, J., Moritz, W., Aballe, L., and Mentes, T. O. (2007). Low energy electron diffraction and low energy electron microscopy microspot I/V analysis of the (4×4)O structure on Ag(111): Surface oxide or reconstruction? *J. Chem. Phys.* 127, 134706. doi:10.1063/1.2779028

Reuter, K. (2016). *Ab initio* thermodynamics and first-principles microkinetics for surface catalysis. *Catal. Lett.* 146, 541–563. doi:10.1007/s10562-015-1684-3

Rocha, T. C. R., Oestereich, A., Demidov, D. V., Hävecker, M., Zafeiratos, S., Weinberg, G., et al. (2012). The silver-Oxygen system in catalysis: New insights by near ambient pressure x-ray photoelectron spectroscopy. *Phys. Chem. Chem. Phys.* 14, 4554. doi:10.1039/c2cp22472k

Schnadt, J., Michaelides, A., Knudsen, J., Vang, R. T., Reuter, K., Lægsgaard, E., et al. (2006). Revisiting the structure of the $p(4×4)$ surface oxide on Ag(111). *Phys. Rev. Lett.* 96, 146101. doi:10.1103/physrevlett.96.146101

Serafin, J. G., Liu, A. C., and Seyedmonir, S. R. (1998). Surface science and the silver-catalyzed epoxidation of ethylene: An industrial perspective. *J. Mol. Catal. A Chem.* 131, 157–168. doi:10.1016/s1381-1169(97)00263-x

Shen, Q., Wu, J., Zhou, F., Song, Y., Dong, W., Wang, X., et al. (2022). A molecular beam-surface apparatus for quantum state-resolved adsorption studies. *Rev. Sci. Instrum.* 93, 013201. doi:10.1063/5.0049178

Shuai, Q., Kaufmann, S., Auerbach, D. J., Schwarzer, D., and Wodtke, A. M. (2017). Evidence for electron-hole pair excitation in the associative desorption of H_2 and D_2 from Au(111). *J. Phys. Chem. Lett.* 8, 1657–1663. doi:10.1021/acs.jpclett.7b00265

Sitz, G. O. (2002). Gas surface interactions studied with state-prepared molecules. *Rep. Prog. Phys.* 65, 1165–1193. doi:10.1088/0034-4885/65/8/202

Vattuone, L., and Okada, M. (2020). "State resolved sticking probability in gas-surface interaction," in *Springer handbook of surface science*. Editors M. Rocca, T. S. Rahman, and L. Vattuone (Cham: Springer), 1053–1084.

Westphal, G., Wallrabe, M., and Schäfer, T. (2020). Unravelling reaction products of styrene oxide adsorbed on ag(111) using rempi-assisted temperature-programmed desorption. *J. Phys. Chem. C* 124, 799–804. doi:10.1021/acs.jpcc.9b10358

White, M. G., and Beuhler, R. J. (2004). State-resolved dynamics of oxygen atom recombination on polycrystalline Ag. *J. Chem. Phys.* 120, 2445–2455. doi:10.1063/1.1637333

Xu, Y., Greeley, J., and Mavrikakis, M. (2005). Effect of subsurface oxygen on the reactivity of the Ag(111) surface. *J. Am. Chem. Soc.* 127, 12823–12827. doi:10.1021/ja043727m